
MRSEGMENTATOR: ROBUST MULTI-MODALITY SEGMENTATION OF 40 CLASSES IN MRI AND CT SEQUENCES

A PREPRINT

Hartmut Häntze^{*1,2}, **Lina Xu**^{*1}, Felix J. Dorfner^{1,3}, Leonhard Donle¹, Felix Busch⁴, Markus R Makowski⁴, Hugo Aerts^{5,6,7}, Daniel Truhn⁸, Avan Kader², Mathias Prokop², Bram van Ginneken², Alessa Hering², Lisa C. Adams⁴, and **Keno K. Bressen**^{†4,9}

¹*Department of Radiology, Charité - Universitätsmedizin Berlin corporate member of Freie Universität Berlin and Humboldt Universität zu Berlin, Hindenburgdamm 30, 12203 Berlin, Germany*

²*Diagnostic Image Analysis Group, Radboud University Medical Center, Geert Grooteplein Zuid 10, 6525 GA Nijmegen, the Netherlands*

³*Athinoula A. Martinos Center for Biomedical Imaging, Massachusetts General Hospital and Harvard Medical School, 149 Thirteenth St, Charlestown, MA 02129, USA*

⁴*Department of Radiology, Klinikum rechts der Isar, Technical University Munich, Ismaninger Str. 22, 81675 Munich, Germany*

⁵*Artificial Intelligence in Medicine (AIM) Program, Mass General Brigham, Harvard Medical School, 221 Longwood Avenue, Boston, MA 02115, USA*

⁶*Departments of Radiation Oncology and Radiology, Dana-Farber Cancer Institute and Brigham and Women's Hospital, 221 Longwood Avenue, Boston, MA 02115, USA*

⁷*Radiology and Nuclear Medicine, CARIM & GROW, Maastricht University, Minderbroedersberg 4-6, 6211 LK Maastricht, Netherlands*

⁸*Department of Diagnostic and Interventional Radiology, University Hospital Aachen, Pauwelsstr. 30, 52074 Aachen, Germany*

⁹*German Heart Center Munich, Technical University Munich, Lazarethstr. 36, 80636 Munich, Germany*

10.05.2024

*These authors contributed equally to this work

†Corresponding author: bressen@dhm.mhn.de

ABSTRACT

Purpose: To introduce a deep learning model capable of multi-organ segmentation in MRI scans, offering a solution to the current limitations in MRI analysis due to challenges in resolution, standardized intensity values, and variability in sequences.

Materials and Methods: The model was trained on 1,200 manually annotated MRI scans from the UK Biobank, 221 in-house MRI scans and 1228 CT scans, leveraging cross-modality transfer learning from CT segmentation models. A human-in-the-loop annotation workflow was employed to efficiently create high-quality segmentations. The model's performance was evaluated on NAKO and the AMOS22 dataset containing 600 and 60 MRI examinations. Dice Similarity Coefficient (DSC) and Hausdorff Distance (HD) was used to assess segmentation accuracy. The model will be open sourced.

Results: The model showcased high accuracy in segmenting well-defined organs, achieving Dice Similarity Coefficient (DSC) scores of 0.97 for the right and left lungs, and 0.95 for the heart. It also demonstrated robustness in organs like the liver (DSC: 0.96) and kidneys (DSC: 0.95 left, 0.95 right), which present more variability. However, segmentation of smaller and complex structures such as the portal and splenic veins (DSC: 0.54) and adrenal glands (DSC: 0.65 left, 0.61 right) revealed the need for further model optimization.

Conclusion: The proposed model is a robust, tool for accurate segmentation of 40 anatomical structures in MRI and CT images. By leveraging cross-modality learning and interactive annotation, the model achieves strong performance and generalizability across diverse datasets, making it a valuable resource for researchers and clinicians. It is open source and can be downloaded from <https://github.com/hhaentze/MRSegmentator>.

Keywords MRI, Segmentation, Cross-Modality, Artificial Intelligence, Radiology

1 Introduction

Artificial intelligence (AI)-based segmentation of medical images has numerous applications, including the calculation of organ volumes, extraction of image-based biomarkers, identification of regions of interest, and provision of anatomical context to improve AI-based diagnosis and radiomics pipelines [1]. For instance, accurate localization of a tumor and determination of its proximity to critical structures can inform treatment planning and prognosis. Considerable progress has been made in developing open-source segmentation models for CT images, most notably TotalSegmentator, which can robustly segment 104 anatomical structures [2]. However, progress in MRI segmentation has been slower due to several challenges. Compared to CT, MRI images have lower resolution and lack standardized intensity values, such as Hounsfield units, making it more difficult for deep learning algorithms to generalize to new data. MRI also has much greater variability arising from the wide range of possible sequences and higher prevalence of artifacts, anisotropic voxel sizes, registration errors, and varying fields of view [3]. Despite these challenges, MRI segmentation is highly valuable as the multiple available sequences provide rich information that can potentially yield more imaging biomarkers and improve diagnostic algorithms compared to CT. While numerous MRI segmentation models exist, many focus only on the brain [4, 5]. Among those that focus on the body, few are openly available, and most target only one or a few organs, such as the kidneys, prostate, or spleen [6, 7, 8]. The increasing availability of large biobanks with extensive MRI data further underscores the need for robust multi-organ MRI segmentation. Detailed segmentation of multiple organs and structures would enable more in-depth research on imaging biomarkers and their associations with disease risk, progression, and treatment response. Furthermore, the development of a comprehensive, open-source multi-organ MRI segmentation model would significantly accelerate research in this field by providing a standardized tool for extracting quantitative data from MRI scans. Such a model could be used to analyze large datasets, identify novel imaging biomarkers, and develop more accurate diagnostic and prognostic algorithms. Additionally, the integration of multi-organ segmentation with other AI techniques, such as radiomics and deep learning-based classification, could lead to more powerful and comprehensive AI-based tools for medical image analysis. To address this need, we have developed MRSegmentator, a deep learning model capable of accurately segmenting 40 different structures in the pelvic, abdominal, and thoracic regions of MRI scans. Our approach leverages cross-modality transfer learning from CT segmentation models, which has shown promise in previous studies [9]. Additionally, we used a human-in-the-loop annotation workflow to establish an efficient annotation pipeline. This approach allowed us to create a model that robustly handles both MRI and CT scans and generalizes well to external datasets. To accelerate research on MRI-based biomarkers and AI diagnostic systems, we have made the MRSegmentator model, training data, and code publicly available at <https://github.com/hhaentze/MRSegmentator>.

2 Materials & Methods

This study was conducted in accordance with the Declaration of Helsinki and approved by the local ethics committee (EA4/062/20). Patient consent was waived due to the retrospective nature of the study.

2.1 Datasets

We utilized four datasets in this study. For training, we used data from the UK Biobank and an in-house dataset. For testing, data from the German National Cohort (NAKO) and the AMOS22 challenge were used.

2.1.1 UK Biobank Dataset

The UK Biobank is a large-scale biomedical database containing genetic and health information from half a million UK participants [10]. We accessed the pancreatic MRI subset (data-field 20202, October 2023), which includes full-body MRI scans of 66,050 participants. Each participant’s MRI data is divided into six regions, from shoulders to knees, with each region covered by four sequences acquired using the Dixon technique: in-phase (IN), opposed-phase (OPP), fat-only (F), and water-only (W) (Image 2). This dataset is highly standardized, with consistent image size, spacing, and participant positioning within each region. We downloaded 1,200 examinations from 50 randomly selected participants,

which were then manually annotated by a radiologist (LX). Access to the UK Biobank dataset is available for scientific research upon request at <https://www.ukbiobank.ac.uk/>.

2.1.2 In-House Dataset

Our in-house dataset consists of abdominal MRI scans from 177 patients with kidney tumors and cysts, yielding 221 scans. Tumor size is below 7 cm for 213 scans and goes up to 13 cm in the remaining 8 scans. This dataset has an approximately equal distribution of T1, T2, and T1-weighted-fat-saturated (T1fs) sequences. It is heterogeneous, as images have been acquired at multiple different scanners with varying intensity distributions, spacings, and sizes. A radiologist (LX) manually annotated 40 classes that were included in most examinations.

2.1.3 TotalSegmentator Dataset

Including CT examinations to the training pipeline can improve segmentation quality for MRI examinations as well [9]. For this purpose we use the TotalSegmentator dataset, which consists of 1228 CT examinations with a wide range of different pathologies, scanners, sequences and institutions [2]. From the 117 segmented structures we select the subset that overlaps with MRSegmentator. Vertebrae, left lung lobes and right lung lobes are combined into joint classes respectively. The dataset can be downloaded from <https://zenodo.org/records/10047292>.

2.1.4 NAKO Dataset

The German National Cohort (NAKO) is a population-based prospective study investigating the causes for the development of major chronic diseases [11]. The study includes whole-body MRI scans of 30,000 participants from the general population. We obtained a subset of 600 MRI scans for testing purposes. The data consists of three T1-GRE modalities (OPP, W, F) for each patient (Table 1), for which two board-certified radiologists manually refined segmentations. The data was used for testing purposes only.

2.1.5 AMOS22 Dataset

The multi-modality abdominal multi-organ segmentation challenge (AMOS22) was held at the MICCAI conference in 2022 [9]. The accessible training and validation sections include 300 CT and 60 MRI images from multi-center, multi-vendor, multi-modality, multi-phase, and multi-disease patients, each with voxel-level annotations of 15 abdominal organs. The AMOS22 dataset was used only for evaluation of our model. We excluded annotations for the bladder, due to label errors in the MRI images (see Appendix A1), and prostate, as it was not part of MRSegmentator’s classes, from our evaluation. The data was used for testing purposes only, it can be accessed at <https://zenodo.org/records/7262581>.

2.2 Annotation Strategy

We employed a human-in-the-loop annotation approach to efficiently create high-quality segmentations for our training data. This iterative process involved the following steps:

1. Pre-segmentation: We generated initial segmentations by running TotalSegmentator [2] on the MRI scans, preceded by several preprocessing steps, such as inversion or histogram equalization [12]. See Figure A2 for an overview of the preprocessing steps. While some of these pre-segmentations were accurate enough to require only minor corrections (e.g., kidneys), TotalSegmentator performed poorly on several organ systems (e.g., muscles or bones), necessitating the creation of these segmentations from scratch.
2. Manual annotation: A radiologist (LX) reviewed and refined the pre-segmentations using MONAI Label and 3D Slicer. Overall, 40 different labels were created, which are detailed in Table 2. Due to the non-isotropic voxel spacing of the axial slices in the UK Biobank data, we combined all vertebrae into a single "spine" label. Furthermore, as MRI provides poor contrast in air-filled organs, the lungs were not annotated on a lobe level.
3. Model retraining: After each set of 50 annotated examinations, we trained a segmentation model based on nnUNet using the updated segmentations [13]. The results of this retrained model served as the basis for the next annotation iteration, progressively improving the quality and efficiency of the manual annotation process.

This human-in-the-loop annotation strategy allowed us to efficiently create a large, high-quality dataset for training MRSegmentator. By iteratively refining the segmentations and retraining the model, we progressively improved the accuracy of the pre-segmentations, reducing the manual effort required in subsequent annotation rounds. Once the annotation process was complete, we trained an nnUNet with five-fold cross-validation on the fully annotated images, resulting in the final model.

Table 1: Data Composition

Training and Validation Data			
	In-House	UKBB	TotalSegmentator
Nr. Participants	171 (m:121, f:56)	50 ¹	1228 (m: 716, f:510)
Nr. Examinations	221(m:150, f:71)	1200 ¹	1228 (m: 716, f:510)
Age [years]	37 - 83 (median=62)	40-69 ¹	15 - 98 (median=65)
Scanner Types	Siemens MAGNETOM Avanto 1.5T Siemens MAGNETOM Vida 3T	1.5 Tesla MRI	20 different models
Sequences	T1 (n=90) T2 (n=64) T1fs post contrast (n=67)	IN (n=300) OPP (n=300) W (n=300) F (n=300)	CT (n=1228)
Test Data			
	NAKO (MRI)	AMOS (MRI)	AMOS (CT)
Nr. Participants	50 (m:25, f:25)	60 (m: 55, f: 45) ²	300 (m: 314, f: 186) ²
Nr. Examinations	600 (m:300, f:300)	60 (m: 55, f: 45) ²	300 (m: 314, f: 186) ²
Age [years]	26-69 (median=52.5)	22-85 (median=50) ²	14-94 (median=54) ²
Scanner Types	3 Tesla MR	3 different models	5 different models
Sequences	T1 GRE OPP (n=200) T1 GRE W (n=200) T1 GRE F (n=200)	MRI (n=60)	CT (n=300)

¹ UK Biobank targets healthy individuals between the ages of 40 and 69 with a target gender-ratio of 1:1.

² Age and sex of the participants of the AMOS22 dataset are given for all 600 images, of which 360 are publicly available with manual annotations.

2.3 Metrics

We evaluated the performance of MRSegmentator using the Dice Similarity Coefficient (DSC) and the Hausdorff Distance (HD). The DSC quantifies the overlap between the predicted segmentation and the ground truth annotation. Its values range from 0 to 1, with 1 indicating perfect overlap between the predicted segmentation and the ground truth. However, the DSC has some limitations, especially for small tubular structures (e.g., adrenal glands, blood vessels), where small segmentation differences can result in significantly lower DSC values compared to those for large structures [14]. Additionally, the DSC does not distinguish between oversegmentation and undersegmentation and does not capture differences in shape. The HD is a boundary-based metric that measures the maximum distance between the predicted segmentation and the ground truth annotation. Since the HD is sensitive to outliers, such as single falsely annotated pixels, we used the 95th percentile variant of the HD. The HD complements the DSC by capturing shape differences and is less sensitive to small segmentation errors. By using both metrics, we provide a comprehensive evaluation of MRSegmentator’s performance, accounting for both overlap and shape differences between the predicted segmentations and the ground truth annotations.

3 Results

3.1 Study Sample Characteristics

The UK Biobank dataset included 1,200 MRI scans from 50 participants between 40 and 69 years of age. The in-house dataset consisted of 221 MRI scans from 177 patients with kidney lesions, ranging in age from 37 to 83 years, with a male-to-female ratio of 2.3:1. The characteristics of the in-house dataset are summarized in Table 2. The TotalSegmentator dataset comprises 1,228 CT scans from patients between 15 and 98 years old, with a male-to-female ratio of 1.4:1. The NAKO dataset included 600 MRI scans from 50 patients, with a median age of 52.5 years and a male-to-female ratio of 1:1. The AMOS22 dataset contained 60 MRI scans and 300 CT scans from multi-center,

Table 2: Overview of different body regions and organs, supported by MRSegmentator

Body Region	Organs
Chest	Heart Left and right lungs Esophagus
Gastrointestinal tract	Liver Spleen Pancreas Gallbladder Stomach Duodenum Small bowel (Jejunum and ileum) Colon
Retroperitoneum	Left and right kidneys Left and right adrenal glands Urinary bladder
Musculoskeletal	Spine Sacrum Left and right hip Left and right femurs Left and right gluteus maximus muscles Left and right gluteus medius muscles Left and right gluteus minimus muscles Left and right autochthonous muscles Left and right iliopsoas muscles
Vessels	Aorta Inferior vena cava Portal/splenic vein Left and right iliac arteries Left and right iliac veins

multi-vendor, multi-modality, multi-phase, and multi-disease patients. The mean age for the MRI and CT scans in the AMOS22 dataset was 48.7 and 53.6 years, respectively, with male-to-female ratios of 1.2:1 for MRI and 1.7:1 for CT.

3.2 Segmentation Performance

MRSegmentator was evaluated on the NAKO and AMOS22 datasets. On the NAKO dataset, the model achieved a mean Dice score of 0.85 ± 0.13 and a mean Hausdorff distance of 6.55 ± 11.90 mm for MRI scans. For the AMOS22 dataset, MRSegmentator yielded a mean Dice score of 0.79 ± 0.11 and a mean Hausdorff distance of 8.29 ± 7.35 mm for MRI scans, demonstrating consistent performance across different datasets. When applied to CT scans from the AMOS22 dataset, the model achieved a mean Dice score of 0.84 ± 0.11 and a mean Hausdorff distance of 7.86 ± 11.12 mm, showcasing its ability to generalize across different imaging modalities. Detailed per-class results can be found in the appendix (Table A1). The highest DSC on the NAKO data was achieved for the left and right lungs, with a value of 0.97 each, and a HD of 3.36 and 3.80. Conversely, the portal/splenic vein and the adrenal glands proved to be the most challenging for the model, with a DSC of 0.54 and a HD of 21.86. On the AMOS22 dataset, the highest DSC was achieved for the spleen with ad DSC of 0.95 and a HD of 2.84. Again, the lowest performance was achieved for the adrenal glands with a DSC of 0.55 and a HD of 9.27. The greatest variability between cases was seen for portal/splenic vein, adrenal glands and gallbladder, where the standard deviation of the DSC ranges from 0.22 to 0.26. Average segmentation quality for males (DSC= 0.87 ± 0.03) is slightly better than for females (DSC= 0.85 ± 0.03) in the external NAKO data ($p=0.03$). This is likely caused by the larger proportion of males in all training data sets. At a categorical level, the greatest differences are measured for the pancreas (Δ DSC=0.11) and left and right adrenal glands (Δ DSC=0.11/0.10). We could not prove this to be significant with Bonferroni correction but, admittedly, the power of our non-corrected one-tailed t-test to detect a medium effect size is comparatively low ($\beta = 0.46$) [15]. The age of the probands does positively correlate with the Dice score ($r=0.32$, $p=0.02$). This could be due to the increased age in the training population, however, might also be a statistical phenomenon caused by a few outliers (Figure A3).

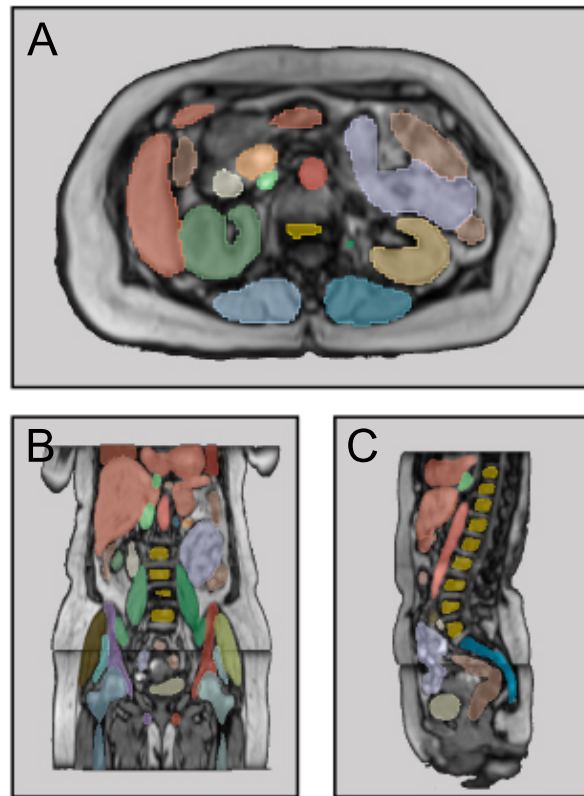


Figure 1: Sample segmentation of MRSegmentator for axial (A), coronal (B) and sagittal (C) views of an MRI image.

Table 3: Segmentation Quality

Validation Data (5-fold Cross-Validation)								
	T1	T2	T1fs	IN	OPP	W	F	CT
DSC	0.84 (0.14)*	0.77 (0.18)	0.85 (0.14)	0.76 (0.17)	0.79 (0.16)	0.82 (0.16)	0.78 (0.16)	0.91 (0.15)
HD [mm]	5.05 (6.09)	6.91 (8.51)	4.63 (5.83)	8.12 (8.45)	7.34 (8.25)	7.07 (9.13)	7.71 (8.43)	7.82 (20.75)
External NAKO Data								
	T1 GRE OPP		T1 GRE W		T1 GRE F			
DSC	0.86 (0.13)		0.84 (0.12)		0.86 (0.13)			
HD [mm]	6.48 (11.86)		5.56 (8.10)		7.60 (13.57)			
External AMOS Data¹								
	MRI		CT		Average NAKO MRI²			
DSC	0.79 (0.11)		0.84 (0.11)		0.81 (0.16)			
HD [mm]	8.29 (7.35)		7.86 (11.12)		4.75 (4.66)			

* Standard deviation is calculated class-wise and between samples

¹ We evaluate on 13 classes of the AMOS data (See Appendix A1)

² Average results of the NAKO data for the same 13 classes

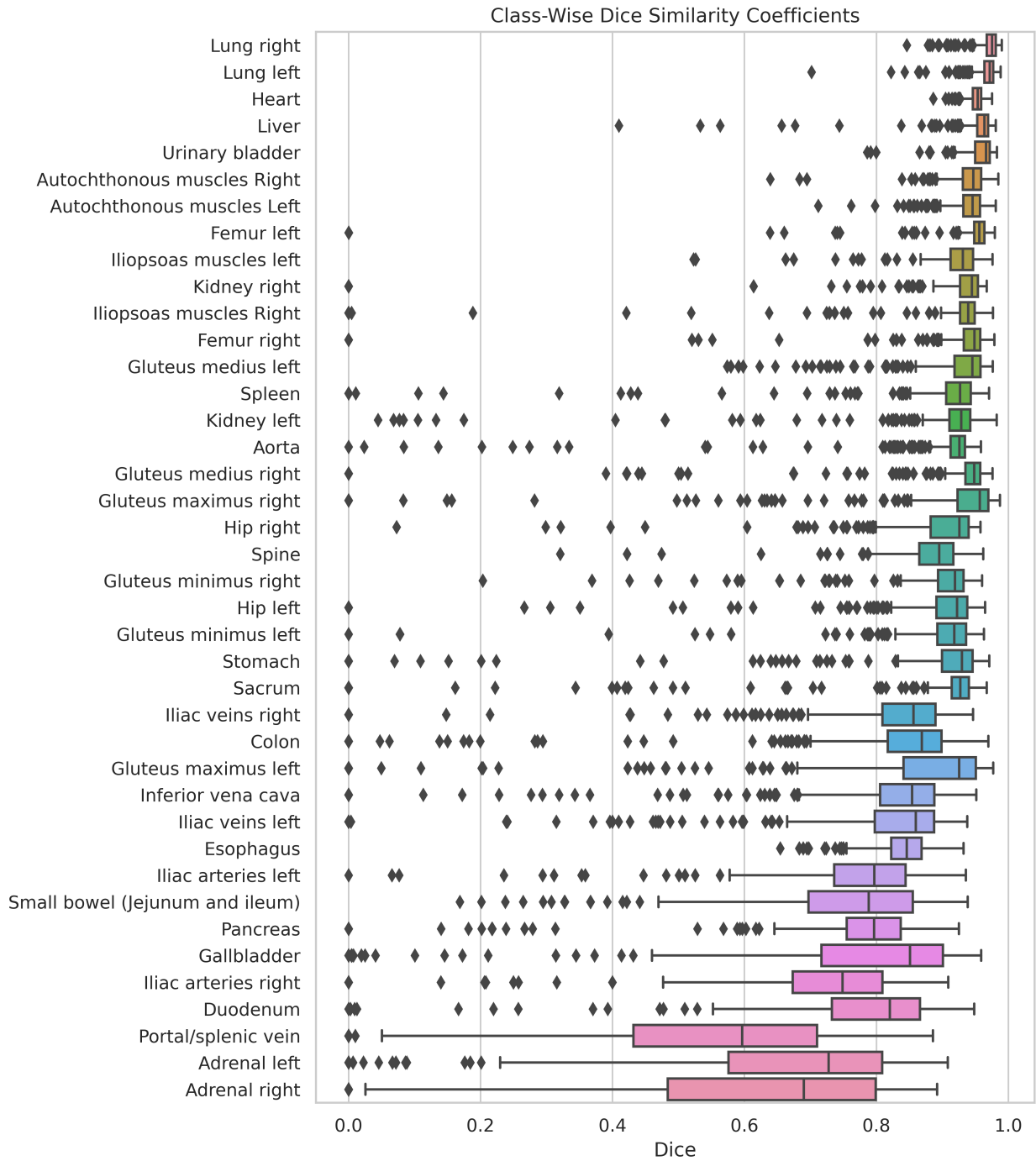


Figure 2: Class-wise dice similarity coefficients of the NAKO dataset

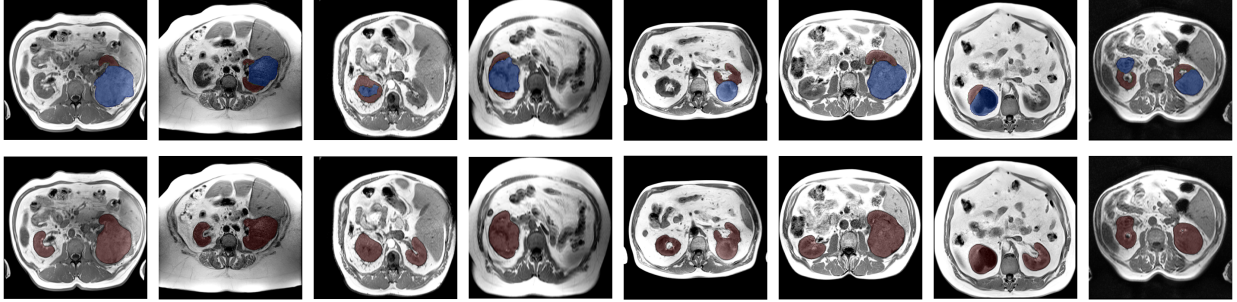


Figure 3: The first row depicts manually annotated kidneys (red) and tumors (blue). The second row shows kidney segmentations of MRSegmentator. Kidneys were localized and segmented accurately even in the presence of large tumors. The missing right kidney in sample four does correctly not result in a segmentation mask.

3.3 Failure Cases and Performance on Pathological Images

While MRSegmentator demonstrated robust performance across various datasets and modalities, some failure cases were observed. The model occasionally struggled with small organs and vessels, such as adrenal glands and porta/splenic vein, resulting in lower Dice scores for these structures. Additionally, segmentation quality varied slightly between different MRI sequence types, with the model performing best on T1 GRE opposed-phase (OPP) sequences ($DSC = 0.86 \pm 0.13$) and worst on Dixon in-phase (IN) sequences ($Dice = 0.76 \pm 0.17$). In few instances the models incorrectly mixes left and right, particularly in the pelvic region. We implemented a postprocessing step, which effectively resolves this for distinct structures but the problem persists for more intricate ones such as blood vessels. Additionally, the model sometimes misses or incorrectly adds structures at the edge of an examination, resulting in a DSC of zero. In these cases few missed voxels can have a large impact on the segmentation metrics. The performance of MRSegmentator on pathological images was also evaluated. In the in-house dataset, which included MRI scans of patients with kidney cancer, the model accurately segmented kidneys of all 8 patients with tumors greater than 7 cm (Figure 3). However, in some instances it appears to oversegment, likely due to the heterogeneous appearance and irregular borders of the tumors. Further investigation is needed to assess the model’s performance on a wider range of pathological conditions.

4 Discussion

In this study, we developed MRSegmentator, a multi-modal, multi-structure segmentation model capable of accurately segmenting 40 organs in MRI and CT images, achieving strong performance across various datasets, sequence types, and modalities. These findings highlight the robustness and generalizability of MRSegmentator in handling diverse imaging data. We have made MRSegmentator the model and code openly available. One of the key advantages of MRSegmentator is its ability to learn from both MRI and CT data simultaneously through cross-modality learning. Although incorporating CT scans into the training pipeline did not significantly improve MRI segmentation performance compared to an MRI-only model, we believe that this approach holds potential to enhance the model’s generalizability to a greater variety of sequences. Moreover, a model that supports multiple modalities can streamline workflows and reduce overhead for researchers working with both MRI and CT data. Compared to existing models, MRSegmentator demonstrates competitive performance. For CT segmentation, our model achieves results comparable to TotalSegmentator [2], which reported a mean Dice score of 0.94. Regarding MRI segmentation, MRSegmentator performs on par with several organ-specific models. For example, a recent study [16] reported a Dice score of 0.95 for liver segmentation in MRI, equal to the DSC achieved by MRSegmentator. Similarly, for the spleen, MRSegmentator comes close to [17] who reported a Dice score of 0.96.

In a study about multi organ segmentation in the NAKO dataset Kart et al. [18] segment liver, spleen, kidneys and pancreas with Dice scores of 0.98, 0.96, 0.98 and 0.89. Correspondingly, our model achieves comparable scores of 0.95, 0.89, 0.89 and 0.75 for NAKO MRI, despite it being an external dataset. On the AMOS dataset, which was annotated by external radiologists, we achieve Dice scores of 0.96, 0.95, 0.95 and 0.81. Granted, we cannot surpass the current leader (stand 07.05.2024) of the AMOS challenge, who achieves a DSC of 0.90 for the 13 labels of the combined CT and MRI test set, while our model has an average of 0.82. However, AMOS is an external dataset for the model and results for it free of overfitting. Although the MRSegmentator does not always surpass specific models on single organ segmentation, the strength of the model is the rich variety of organs and robustness across different MR and CT sequences. This simplicity in use likely will outweigh slightly inferior performance compared to specialized models.

However, our study has limitations. First, the same radiologist annotated our training and validation data using a "human-in-the-loop" approach, potentially introducing annotation bias. For some structures, such as duodenum, it can be challenging to define beginning and end, resulting in a low inter-observer agreement. The inter-observer agreement of the pancreas, for example, can have a Dice score as low as 0.85 [18]. Although the model's strong performance on the external AMOS22 dataset suggests that this bias may not significantly impact generalizability for most structures, multiple annotators could have mitigated this issue. Second, the inherent complexity of MRI images poses challenges in distinguishing target structures from surrounding tissue, particularly for small structures. While MRSegmentator produces segmentations that visually are sometimes as accurate or even better than human annotations, voxel-based metrics such as Dice and Hausdorff distance may not fully capture the quality of these segmentations when they deviate from the predefined ground truth. It is important to note that the acceptable level of accuracy and the impact of under- or over-segmentation may vary depending on the specific application. The Dice coefficient, while widely used, does not fully represent these nuances [14]. Furthermore, the correction effort required to refine the segmentations is another critical factor to consider. For example, if an application requires 'perfect' segmentation, a model that makes small errors throughout the image (e.g., with a Dice score of 0.9) may require several minutes of correction time. In contrast, a model that makes one large error (e.g., with a Dice score of 0.85) may only require a few seconds of correction, making it a more practical choice despite having a lower Dice score. In conclusion, MRSegmentator represents an advance in multi-modal, multi-structure segmentation, demonstrating strong performance and generalizability across diverse datasets. By leveraging cross-modality learning and interactive annotation, our model can accurately segment 40 classes in MRI and CT images, making it a valuable tool for researchers and clinicians. The open-source availability of MRSegmentator will facilitate its adoption and contribute to the advancement of automated segmentation techniques in medical imaging research. As the field progresses, it will be crucial to consider application-specific requirements and the trade-offs between accuracy metrics and practical usability to develop models that best serve the needs of researchers and clinicians.

Acknowledgements

Much of the computation resources required for this research was performed on computational hardware generously provided by the Charité HPC cluster (https://www.charite.de/en/research/research_support_services/research_infrastructure/science_it/#c30646061). This work was in large parts funded by the Wilhelm Sander Foundation. Funded by the European Union. Views and opinions expressed are however those of the author(s) only and do not necessarily reflect those of the European Union or European Health and Digital Executive Agency (HADEA). Neither the European Union nor the granting authority can be held responsible for them.

References

- [1] Robert J Gillies, Paul E Kinahan, and Hedvig Hricak. Radiomics: images are more than pictures, they are data. *Radiology*, 278(2):563–577, 2016. doi:10.1148/radiol.2015151169.
- [2] Jakob Wasserthal, Hanns-Christian Breit, Manfred T Meyer, Maurice Pradella, Daniel Hinck, Alexander W Sauter, Tobias Heye, Daniel T Boll, Joshy Cyriac, Shan Yang, et al. Totalsegmentator: Robust segmentation of 104 anatomic structures in ct images. *Radiology: Artificial Intelligence*, 5(5), 2023. doi:10.1148/ryai.230024.
- [3] Geert Litjens, Thijs Kooi, Babak Ehteshami Bejnordi, Arnaud Arindra Adiyoso Setio, Francesco Ciompi, Mohsen Ghafoorian, Jeroen Awm Van Der Laak, Bram Van Ginneken, and Clara I Sánchez. A survey on deep learning in medical image analysis. *Medical image analysis*, 42:60–88, 2017. doi:10.1016/j.media.2017.07.005.
- [4] Yuankai Huo, Zhoubing Xu, Yunxi Xiong, Katherine Aboud, Prasanna Parvathaneni, Shunxing Bao, Camilo Bermudez, Susan M Resnick, Laurie E Cutting, and Bennett A Landman. 3d whole brain segmentation using spatially localized atlas network tiles. *NeuroImage*, 194:105–119, 2019. doi:10.1016/j.neuroimage.2019.03.041.
- [5] Andriy Myronenko. 3d mri brain tumor segmentation using autoencoder regularization. In *Brainlesion: Glioma, Multiple Sclerosis, Stroke and Traumatic Brain Injuries: 4th International Workshop, BrainLes 2018, Held in Conjunction with MICCAI 2018, Granada, Spain, September 16, 2018, Revised Selected Papers, Part II 4*, pages 311–320. Springer, 2019. doi:10.1038/s41592-023-02151-z.
- [6] Lisa C Adams, Marcus R Makowski, Günther Engel, Maximilian Rattunde, Felix Busch, Patrick Asbach, Stefan M Niehues, Shankeeth Vinayahalingam, Bram van Ginneken, Geert Litjens, et al. Prostate158-an expert-annotated 3t mri dataset and algorithm for prostate cancer detection. *Computers in Biology and Medicine*, 148:105817, 2022. doi:10.1016/j.combiomed.2022.105817.
- [7] Yuankai Huo, Jiaqi Liu, Zhoubing Xu, Robert L Harrigan, Albert Assad, Richard G Abramson, and Bennett A Landman. Robust multicontrast mri spleen segmentation for splenomegaly using multi-atlas segmentation. *IEEE Transactions on Biomedical Engineering*, 65(2):336–343, 2017. doi:10.1109/TBME.2017.2764752.

-
- [8] Taro Langner, Andreas Östling, Lukas Maldonis, Albin Karlsson, Daniel Olmo, Dag Lindgren, Andreas Wallin, Lowe Lundin, Robin Strand, Håkan Ahlström, et al. Kidney segmentation in neck-to-knee body mri of 40,000 uk biobank participants. *Scientific reports*, 10(1):20963, 2020. doi:10.1038/s41598-020-77981-4.
- [9] Yuanfeng Ji, Haotian Bai, Chongjian Ge, Jie Yang, Ye Zhu, Ruimao Zhang, Zhen Li, Lingyan Zhanng, Wanling Ma, Xiang Wan, et al. Amos: A large-scale abdominal multi-organ benchmark for versatile medical image segmentation. *Advances in Neural Information Processing Systems*, 35:36722–36732, 2022. doi:10.48550/arXiv.2206.08023.
- [10] Thomas J Littlejohns, Jo Holliday, Lorna M Gibson, Steve Garratt, Niels Oesingmann, Fidel Alfaro-Almagro, Jimmy D Bell, Chris Boulton, Rory Collins, Megan C Conroy, et al. The uk biobank imaging enhancement of 100,000 participants: rationale, data collection, management and future directions. *Nature communications*, 11(1):2624, 2020. doi:10.1038/s41467-020-15948-9.
- [11] German National Cohort (GNC) Consortium geschaeftsstelle@ nationale-kohorte. de. The german national cohort: aims, study design and organization. *European journal of epidemiology*, 29(5):371–382, 2014. doi:10.1007/s10654-014-9890-7.
- [12] Hartmut Häntze, Lina Xu, Leonhard Donle, Felix J. Dorfner, Alessa Hering, Lisa C. Adams, and Keno K. Bressem. Improve cross-modality segmentation by treating mri images as inverted ct scans. *arXiv*, 2024. doi:10.48550/ARXIV.2405.03713.
- [13] Fabian Isensee, Paul F Jaeger, Simon AA Kohl, Jens Petersen, and Klaus H Maier-Hein. nnu-net: a self-configuring method for deep learning-based biomedical image segmentation. *Nature methods*, 18(2):203–211, 2021. doi:10.1038/s41592-020-01008-z.
- [14] Lena Maier-Hein, Annika Reinke, Patrick Godau, Minu D Tizabi, Florian Buettner, Evangelia Christodoulou, Ben Glocker, Fabian Isensee, Jens Kleesiek, Michal Kozubek, et al. Metrics reloaded: recommendations for image analysis validation. *Nature methods*, pages 1–18, 2024. doi:10.1038/s41592-023-02151-z.
- [15] Franz Faul, Edgar Erdfelder, Albert-Georg Lang, and Axel Buchner. G* power 3: A flexible statistical power analysis program for the social, behavioral, and biomedical sciences. *Behavior research methods*, 39(2):175–191, 2007. doi:10.3758/bf03193146.
- [16] Md Sakib Abrar Hossain, Sidra Gul, Muhammad EH Chowdhury, Muhammad Salman Khan, Md Shaheenur Islam Sumon, Enamul Haque Bhuiyan, Amith Khandakar, Maqsd Hossain, Abdus Sadique, Israa Al-Hashimi, et al. Deep learning framework for liver segmentation from t 1-weighted mri images. *Sensors*, 23(21):8890, 2023. doi:10.3390/s23218890.
- [17] Arman Sharbatdaran, Dominick Romano, Kurt Teichman, Hreedi Dev, Syed I Raza, Akshay Goel, Mina C Moghadam, Jon D Blumenfeld, James M Chevalier, Daniil Shimonov, et al. Deep learning automation of kidney, liver, and spleen segmentation for organ volume measurements in autosomal dominant polycystic kidney disease. *Tomography*, 8(4):1804–1819, 2022. doi:10.3390/tomography8040152.
- [18] Turkay Kart, Marc Fischer, Thomas Küstner, Tobias Hepp, Fabian Bamberg, Stefan Winzeck, Ben Glocker, Daniel Rueckert, and Sergios Gatidis. Deep learning-based automated abdominal organ segmentation in the uk biobank and german national cohort magnetic resonance imaging studies. *Investigative Radiology*, 56(6):401–408, 2021. doi:10.1097/RLI.0000000000000755.

5 Appendix

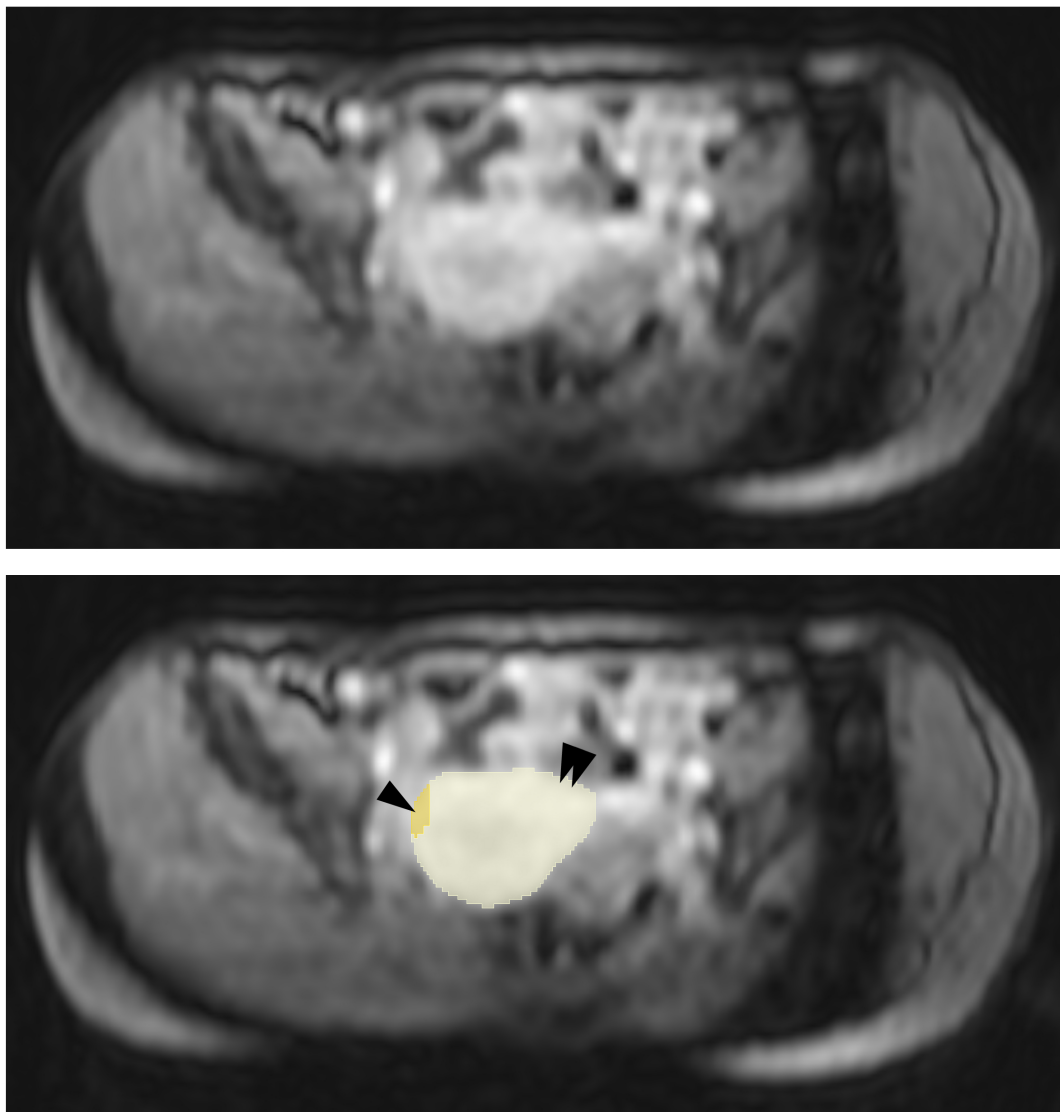


Figure A1: The AMOS22 dataset contains only two MRI examinations with bladder annotations. Of these two annotations, one incorrectly combines the bladder (yellow) with the uterus (beige). Consequently, we exclude the label "bladder" from our evaluation of the AMOS22 dataset.

Table A1: Comparison of DSC and HD for NAKO, AMOS22 (MRI), and AMOS22 (CT). Note that not all 40 classes supported by MRSegmentator are present in the AMOS22 dataset.

Structure	NAKO (MRI)		AMOS22 (MRI)		AMOS22 (CT)	
	DSC	HD	DSC	HD	DSC	HD
Liver	0.95	4.57	0.96	4.26	0.96	5.46
Heart	0.95	3.36
Lung left	0.97	3.36
Lung right	0.97	3.80
Esophagus	0.84	2.71	0.64	13.48	0.80	8.43
Spleen	0.89	4.79	0.95	2.84	0.95	3.92
Pancreas	0.75	8.86	0.81	7.91	0.81	9.26
Gallbladder	0.74	5.37	0.76	8.20	0.81	9.18
Stomach	0.89	5.08	0.86	9.34	0.89	12.81
Duodenum	0.76	7.81	0.58	18.44	0.68	14.38
Small bowel (Jejunum and ileum)	0.75	14.08
Colon	0.81	8.61
Kidney left	0.88	4.28	0.95	3.08	0.94	3.51
Kidney right	0.90	3.35	0.95	3.57	0.95	3.24
Adrenal left	0.65	4.71	0.55	9.27	0.71	5.86
Adrenal right	0.61	3.82	0.56	7.78	0.70	5.97
Urinary bladder	0.95	3.01
Spine	0.89	2.99
Sacrum	0.87	3.61
Hip left	0.89	9.64
Hip right	0.89	11.95
Femur left	0.94	8.95
Femur right	0.93	5.59
Gluteus maximus left	0.85	7.62
Gluteus maximus right	0.91	10.88
Gluteus medius left	0.92	2.78
Gluteus medius right	0.90	2.91
Gluteus minimus left	0.88	2.73
Gluteus minimus right	0.89	2.35
Autochthonous muscles Left	0.94	3.38
Autochthonous muscles Right	0.94	3.20
Iliopsoas muscles left	0.92	6.88
Iliopsoas muscles Right	0.91	8.16
Aorta	0.90	2.58	0.90	13.26	0.93	13.51
Inferior vena cava	0.81	3.85	0.82	6.33	0.84	6.63
Portal/splenic vein	0.54	21.86
Iliac arteries left	0.77	18.67
Iliac arteries right	0.72	7.77
Iliac veins left	0.80	17.36
Iliac veins right	0.82	4.48
Mean	0.85	6.55	0.79	8.29	0.84	7.86

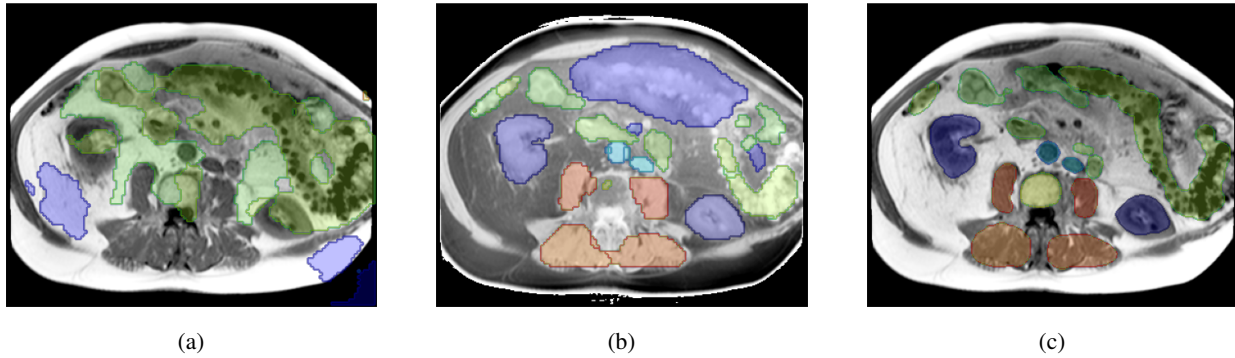


Figure A2: Segmentation quality of TotalSegmentator on a T1-weighted MRI image (a) compared to an inverted version (b) and a refined ground truth (c).

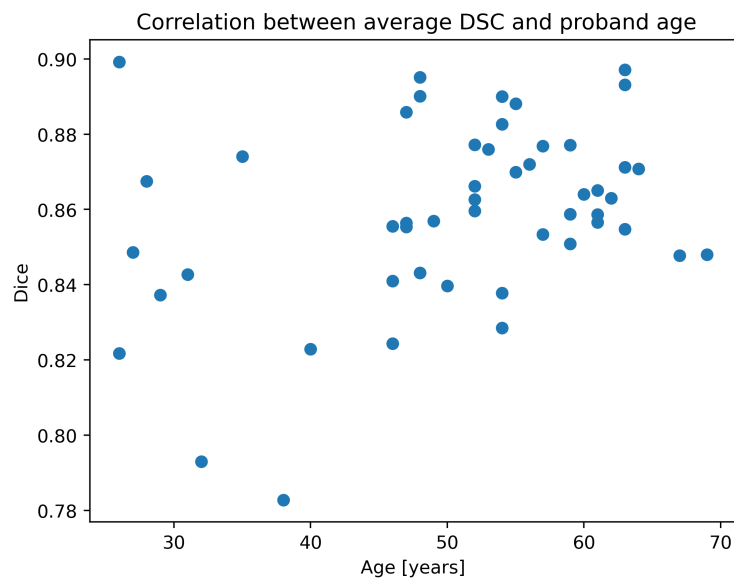


Figure A3: The Dice similarity coefficient correlates positively with proband age ($r=0.33$, $p=0.02$).